Persico, L.P. et al., 2021, Late Quaternary geochronologic record of soil formation and erosion: Effects of climate change on Mojave Desert hillslopes (Nevada, USA): Geology, https://doi.org/10.1130/G49270.1

Soil Characterization Methods

Field Mapping and Sample Collection

The Nipton Hills consist of a series of basins composed of crystalline early Proterozoic bedrock (Miller and Wooden, 1993). The nearest weather recording station, 22 km to the east and 1080 m ASL (US COOP station, Searchlight, NV) receives 196 mm of mean annual precipitation (MAP) and the mean annual temperature (MAT) of 17.3°C. Estimated MAP at the study area (1400 m ASL) is ~ 250 mm (McAuliffe, 2016). Precipitation is distinctly bimodal, with a pronounced cool-season peak from November through March and a summer monsoonal peak in July through September. Precipitation data in Figure 1 is from the Prism Climate Group, Oregon State University (2004). A digital elevation model (DEM) and orthophoto were constructed using structure from motion (SFM) of high overlap unmanned aerial vehicle imagery (Colomina and Molina, 2014). An eight-unit surficial geologic map was created by field mapping. Field identification of geomorphic units was aided by observations of vegetation type, soil morphology, and the high-resolution DEM and orthophoto. Standard soil-geomorphic properties were described (Birkeland, 1999) for 21 locations in the study area. Three locations selected for detailed soil analyses: (1) a north-facing hillslope with a well-developed soil in thick colluvium, (2) a prominent, isolated remnant of a similar colluvial deposit and associated soil on the south-facing slope, and (3) a prominent, well-preserved terrace remnant along the axial drainage (Table S1). At these locations, 0.1-1.0 kg samples were collected from each soil horizon for OSL, XRF, and particle size analyses. Rock samples were also collected to characterize bedrock variability throughout the study area. Cover of the ground surface by canopies of perennial plant species was measured by point-intercept sampling at 10 hillslope locations. Detailed vegetation data and mapping are included in a separate paper.

Table S1. Soil profile descriptions and locations

Horizon	Depth (cm)	MC (dry)	Struc[a]	Dry C[b]	Wet C[c]	Texture	Texture$_d$	Gravel%[e]	HCl[f]	$CaCO_3$ Stage[g]
Soil Profile ON - N aspect, thick colluvial mantle (35.45716° N, 115.17670° W)										
A1	0-1	10YR 3/3	1, f, pl	so	ns, sp	44 – 48 – 8	L	5-10	ne	0
A2	1-4	10YR 7/4	lo	so	ns, sp	34 – 55 – 11	SiL	< 5	ne	0
B	4-21	10YR 6/4	f-c, gr	so	s, p	27 – 57 – 16	SiL	30	ne (matrix)	0
Btk1	21-71	7.5-10YR 6/6	2, m, sbk	sh	s, p	26 – 56 – 18	SiL	60-75	se (upper) ve (lower)	I
Btk2	71-121+	7.5YR 6/6	m	h	s, p	23 -59 – 18	SiL	-	se	I
Soil Profile OS - S aspect, thick colluvial mantle remnant (35.45932° N, 115.17541° W)										
V	0-1	10YR 5/4	1, f, pl	so	ns, np	57 – 35 – 8	SL	-	ne	0
A	1-10	10YR 5/4	1, f, gr-nc	so	ss, sp	30 – 52 – 18	SiL	>75	ne	0
AB	10-25	10YR 6/6	lo	so	s, p	36 – 49 – 15	L	>75	e	I
Bk	25-45	7.5YR 6/6	1, m, sbk	sh	ss, sp	33 – 52 - 15	SiL	<5	se	I
Btk	45-70	7.5YR 5/6	2, m, sbk	sh	ss, sp	32 – 53 – 15	SiL	<5	e	I
B'k	70-85	10YR 5/6	m	sh	ss, sp	34 – 52 – 14	SiL	75	e	0
B'k2	85-125+	10YR 6/6	lo	so	ss, sp	40 – 48 – 12	L	75	e	0
Soil Profile OT - Holocene alluvial terrace (35.5546° N, 115.18237° W)										
A	0-0.5	10YR 6/4	lo		ns, np		LS	-	ne	
AB	0.5-5	10YR 6/4	f-c, gr		ns, np	64-31-5	SL	25	ne	
Bk1	5-20	10YR 6/4	1, f-m, gr	so	ss, np	65-30-5	SL	>35	ne (matrix)	
Bk2	20-38	10YR 6/4	f, gr	so	ss, np	64-30-5	SL		e (matrix)	I
Bk3	38-70+	10YR 6/3	lo		ns, np	80-19-1	S		e (matrix)	

[a]Structure – 1: weak; 2: moderate; f: fine; m: medium; c: coarse; sbk: subangular blocky; pl: platy; gr: granular; ve: vesicular; ma: massive, lo: loose & non-coherent.

[b]Dry Consistence – so: soft; sh: slightly hard; h: hard.

[c]Wet Consistence – ns: non-sticky; ss: slightly sticky; s: sticky; np: non-plastic, sp: slightly plastic; p: plastic.

[d]Textural class – S: sand; LS: loamy sand; SL: sandy loam; L: loam; SCL: sandy clay loam; CL: clay loam; SiL: silt loam; SiCL: silty clay loam

[e]Rock + gravel (visual estimate).

[f]HCl reaction (effervescence) – ne: non-effervescent; e: slightly effervescent; se: strongly effervescent; ve: violently effervescent.

[g]Carbonate accumulation stage (Gile et al., 1966) – 0 = absent; I–IV = Stages I–IV.

[h]Horizon lower boundary – a: abrupt; c: clear; g: gradual; s: smooth, w: wavy.

OSL Sample Collection

Eight samples for OSL dating were collected from three sites in the Nipton Hills. OSL samples were collected from the soil profiles in colluvium on south aspect (LP-01, LP-02, LP-03) and north aspect (LP-04, LP-05, LP-06) hillslopes and alluvium from a 1.5m axial stream terrace (LP-07, LP-08). Methods for sample collection, processing and age determination are outlined below. OSL provides an age estimate of the time since sediment was last exposed to light (Huntley et al., 1985). Therefore, special considerations were followed to ensure that the sediment intervals targeted for OSL dating were not exposed to light during sample collection. Prior to sampling, vertical profiles were dug into the terrace alluvium and representative sites in the south- and north-facing hillslope colluvium. These profiles were cleaned off and described for sediment and soil structures prior to identifying the target intervals for OSL sampling. Due to the finer-grained nature of the sandy-gravel of the terrace alluvium, we were able to use traditional sampling methods (e.g. Nelson et al., 2015) and pound metal pipes horizontally into the sediment (LP-07 USU-2644, LP-08 USU-2645). The colluvial deposits on the hillslopes however were too coarse to allow us to drive a tube into the finer matrix between the clasts. For these sites we collected the samples at night using red-light headlamps (Kenworthy et al., 2014; Nelson et al., 2015). During night-time sampling, the exposures were cleared back to remove light-exposed sediments and then the fine fraction was extracted from between larger clasts and stored in light-safe container for transport. For both sampling methods, we collected representative rocks and sediment from around each target interval for dose rate determination and measurement of water content.

Sample Processing

OSL samples were processed and analyzed at the Utah State University Luminescence Laboratory in Logan, Utah. Samples were opened under dim amber light (~590 nm) and sieved to two grainsize fractions (63-150 μm and 250-355 μm) to help identify different sourced sediment. The alluvial terrace sample was sieved to 90-150 μm. Quartz sediment in each grain-size fraction was isolated by using 10% hydrochloric acid (HCl) and 5% sodium hypochlorite (bleach) to dissolve carbonates and organic material and sodium polytungstate (2.7 g/cm^3) to remove heavy minerals. Feldspar and other non-quartz minerals were removed using three 30-minute etchings in concentrated hydrofluoric acid (47% HF) followed by hydrochloric acid (45%

HCl) to prevent formation of fluorite precipitates (See Rittenour et al., 2005 for details). Purity of the samples was checked using infrared (IR) stimulation; all aliquots with an IR response signal to background ratio of > 2.0 were rejected and not used for age calculation.

Dose Rate Determination

Key to calculating the OSL age of a sample is determination of the rate of radiation exposure the sample received during burial. The concentrations of the K, Rb, Th, and U radioisotopes were analyzed using ICP-MS and ICP-AES techniques on representative sediment and rock subsamples collected from the OSL target intervals (Table S2). These concentrations were converted to dose rate using conversation factors (Guérin et al., 2011) and corrected for attenuation due to the specific grain-size fractions analyzed (Brennan, 2003) and water content (Aitken, 1998). The beta dose rate was calculated from the radio-elemental concentrations of the fine sediment fraction only, while the gamma dose rate was calculated as a function of the percent of fine sediment and rock/cobble/pebble content (see Table S3). Total dose-rate values include cosmic contribution by using sample depth, elevation, and longitude/latitude following Prescott and Hutton (1994). Dose-rate uncertainties were calculated in quadrature using the methods of Aitken and Alldred (1972) and Aitken (1976, 1985) and include uncertainty in the elemental concentrations related to ICP detection limits (following Rittenour et al., 2005), moisture content variability (5±2% weight percent water content used), 3% uncertainty for dose-rate conversion (Murray and Olley, 2002) and 10% uncertainty in cosmic dose.

Table S2. Dose Rate Information

Sample num.	USU num.	Depth (m)	Fraction[1]	K (%)[2]	Rb (ppm)[2]	Th (ppm)[2]	U (ppm)[2]	Cosmic (Gy/kyr)
LP-01	USU-2230	0.18-0.28	Fines (45%)	2.76±0.07	87.5±3.5	10.4±0.9	2.4±0.2	0.26±0.03
			Rocks (55%)	4.91±0.12	224.0±9.0	37.4±3.4	1.9±0.1	
LP-02	USU-2231	0.6-0.7	Fines (60%)	3.41±0.09	178.0±7.1	24.3±2.2	3.1±0.2	0.25±0.02
			Rocks (40%)	3.48±0.09	158.5±6.3	31.3±2.8	2.1±0.2	
LP-03	USU-2232	0.95-1.00	Fines (55%)	2.89±0.07	147.0±5.9	23.7±2.1	2.6±0.2	0.24±0.02
			Rocks (45%)	4.16±0.10	179.0±7.2	39.8±3.6	3.0±0.2	
LP-04	USU-2233	0.2-0.3	Fines (35%)	3.30±0.08	174.5±7.0	23.8±2.1	2.4±0.2	0.26±0.03
			Rocks (65%)	4.80±0.12	234.0±9.4	32.3±2.9	1.6±0.1	
LP-05	USU-2234	0.7-0.8	Fines (35%)	3.32±0.08	172.0±6.9	26.2±2.4	2.5±0.2	0.24±0.02
			Rocks (65%)	4.32±0.11	223.0±8.9	24.7±2.2	1.7±0.1	
LP-06	USU-2235	0.15-0.23	Fines (80%)	1.81±0.05	98.9±4.0	11.5±1.0	2.6±0.2	0.26±0.03
			Rocks (20%)	1.63±0.04	136.0±5.4	8.3±0.7	1.8±0.1	
LP-07	USU-2644	0.30-0.34	Sand (50%)	3.46±0.09	157.5±6.3	27.8±2.5	2.5±0.2	0.26±0.03
			Pebble (50%)	4.25±0.11	175.0±7.0	19.2±1.7	1.9±0.1	
LP-08	USU-2645	0.14-0.17	Sand (40%)	3.57±0.09	144.5±5.8	29.6±2.7	2.5±0.2	0.26±0.03
			Pebble (40%)	4.20±0.11	179.0±7.2	27.4±2.5	2.4±0.2	
			Cobble (20%)	3.39±0.08	177.5±7.1	42.3±3.8	4.6±0.3	

[1] Weight % (in parentheses) proportions of the fines/sand and rocks/pebble/cobbles in each representative dose-rate sample collected from the sediments surrounding each OSL sample.

[2] Radio-elemental concentrations of the sediment surrounding each OSL sample, determined using ICP-MS and ICP-AES techniques.

Optical Measurements

OSL samples were analyzed following the single-aliquot regenerative dose (SAR) technique of Murray and Wintle (Murray and Wintle, 2000) of quartz sand (1-2 mm diameter for 63-150µm and 5 mm diameter for 250-355 µm fraction). Optical measurements were performed on Risø TL/OSL Model DA-20 readers, with stimulation by blue-green light emitting diodes (LED, 470±30 nm) and the luminescence signal was detected through 7.5-mm UV filters (U-340) over 40-50 seconds (250 channels) at 125ºC with LED diodes at 40 mW/cm^2 power. Luminescence signals were calculated by subtracting the average of the last 5 seconds (background signal) from the sum of first 0.7 seconds (4 channels) of signal. The luminescence signals show rapid decay dominated by the fast component of the signal, essential for accurate quartz OSL results (Wintle and Murray, 2006). Average 'Fast ratios' (Durcan and Dulller, 2011) and luminescence sensitivity (photon counts produced per dose of applied radiation) for the very

fine sand fraction were notably higher than those from the fine to medium sand fraction (Figure S1 and S2).

Table S3. Dose Rate contributions

Sample num.	USU num.	Grain size (μm)	Beta[1] (Gy/kyr)	Gamma[2] (Gy/kyr)	Cosmic[3] (Gy/kyr)	Total DR[4] (Gy/kyr)
LP-01	USU-2230	63-150	2.53±0.10	2.30±0.09	0.26±0.03	5.10±0.21
		250-355	2.30±0.09			4.86±0.20
LP-02	USU-2231	63-150	3.42±0.16	2.32±0.11	0.25±0.02	5.99±0.28
		250-355	3.08±0.15			5.66±0.27
LP-03	USU-2232	63-150	2.96±0.15	2.51±0.12	0.24±0.02	5.71±0.28
		250-355	2.67±0.13			5.42±0.27
LP-04	USU-2233	63-150	3.24±0.15	2.53±0.12	0.26±0.03	6.04±0.28
		250-355	2.93±0.14			5.72±0.27
LP-05	USU-2234	63-150	3.32±0.16	2.29±0.11	0.24±0.02	5.85±0.27
		250-355	3.00±0.14			5.53±0.26
LP-06	USU-2235	63-150	1.90±0.09	1.17±0.05	0.26±0.03	3.33±0.16
		250-355	1.71±0.07			3.15±0.13
LP-07	USU-2644	90-150	3.42±0.14	2.21±0.09	0.26±0.03	5.89±0.23
LP-08	USU-2645	90-150	3.54±0.17	2.61±0.13	0.26±0.03	6.42±0.31

[1] Beta dose rate based on the radio-elemental concentrations of the sand/fines from the representative sample of the sediment surrounding the OSL sample (see Table S1). This dose rate includes attenuation from 5±2% weight percent water content (following Aitken, 1985 for beta dose), is scaled by grain size following Brennan (2003) and is based on conversion factors of Guérin et al. (2011).

[2] Gamma dose rate based on the radio-elemental concentrations of both the sand/fines and the rock/pebbles/cobbles in their weight-percent proportions (see Table S1). This dose rate includes attenuation from 5±2% weight percent water content (following Aitken and Xie 1990 and Aitken 1985 for gamma dose) and is based on conversion factors of Guérin et al. (2011).

[3] Contribution of cosmic radiation to the dose rate was calculated by using sample depth, elevation, and longitude/latitude following Prescott and Hutton (1994).

[4] Total dose rate is derived from summed contributions from the beta, gamma and cosmic dose rates for the grain-size fraction of each sample.

Equivalent Dose (De) and Error Calculation

We analyzed 20 to 42 aliquots (subsamples, approximately 50-100 sand grains) per sample to calculate the equivalent dose (De) of radiation the sample received during burial to determine the OSL ages. De values were calculated using interpolation onto dose-response plots fit with saturating-exponential and saturating-exponential plus linear fits to the given regenerative dose points. Data from aliquots were rejected and not used in age calculation if they had evidence of feldspar contamination, corrected signals from repeated doses >20% of unity, recuperation of the zero-dose point >10% of the natural signal, or De greater than the highest regenerative dose given. OSL ages (Table S4) were calculated using the central age

model (CAM) of Galbraith and Roberts (2012) on all samples except the 63-150 μm fraction of LP-06 (USU-2235), which was calculated using a Minimum Age Model (MAM, Galbraith and Roberts, 2012) due to large inter-aliquot scatter (See Figure S2). Errors on De and age estimates are reported at 2-sigma standard error and include errors related to instrument calibration, and dose rate and equivalent dose calculations and were calculated in quadrature using the methods of Aitken and Alldred (1972).

Table S4. Optically Stimulated Luminescence (OSL) Age Information

Sample num.	USU num.	Grain size (μm)	Num. of aliquots[1]	Dose rate (Gy/ka)	Equivalent Dose ± 2σ (Gy)	OSL age ± 2σ (ka)	Age Model[2]
LP-01	USU-2230	63-150	14 (29)	5.10 ± 0.21	67.90 ± 9.14	**13.33 ± 2.09**	**CAM**
LP-01	USU-2230	250-355	15 (31)	4.86 ± 0.20	88.11 ± 18.98	**18.12 ± 4.17**	**CAM**
LP-02	USU-2231	63-150	14 (32)	5.99 ± 0.28	110.57 ± 19.24	**18.46 ± 3.68**	**CAM**
LP-02	USU-2231	250-355	16 (42)	5.66 ± 0.27	168.88 ± 20.21	**29.85 ± 4.60**	**CAM**
LP-03	USU-2232	63-150	19 (28)	5.71 ± 0.28	107.61 ± 17.25	**18.84 ± 3.54**	**CAM**
LP-03	USU-2232	250-355	13 (25)	5.42 ± 0.27	125.47 ± 32.64	**23.15 ± 6.43**	**CAM**
LP-04	USU-2233	63-150	15 (24)	6.04 ± 0.28	63.45 ± 6.26	**10.51 ± 1.45**	**CAM**
LP-04	USU-2233	250-355	14 (20)	5.72 ± 0.27	47.32 ± 5.42	**8.27 ± 1.24**	**CAM**
LP-05	USU-2234	63-150	12 (32)	5.85 ± 0.27	87.23 ± 9.25	**14.91 ± 2.14**	**CAM**
LP-05	USU-2234	250-355	11 (14)	5.53 ± 0.26	88.83 ± 19.81	**16.07 ± 3.91**	**CAM**
LP-06	USU-2235	63-150	12 (41)	3.33 ± 0.16	9.54 ± 2.89	**2.86 ± 0.91**	**MAM**
LP-06	USU-2235	250-355	11 (31)	3.15 ± 0.13	7.48 ± 1.83	**2.38 ± 0.61**	**CAM**
LP-07	USU-2644	90-150	12 (24)	5.89 ± 0.23	20.64 ± 1.28	**3.51 ± 0.36**	**CAM**
LP-08	USU-2645	90-150	19 (24)	6.42 ± 0.31	20.77 ± 3.66	**3.24 ± 0.65**	**CAM**

[1] Age analysis using the single-aliquot regenerative-dose procedure of Murray and Wintle (2000) on 1-2 mm (63-150μm fraction), or 5-mm (250-355μm fraction) aliquots of quartz sand. Number of aliquots used in age calculation and number of aliquots analyzed in parentheses.

[2] Equivalent dose (De) calculated using the Central Age Model (CAM) or the Minimum Age Model (MAM) of Galbraith and Roberts (2012).

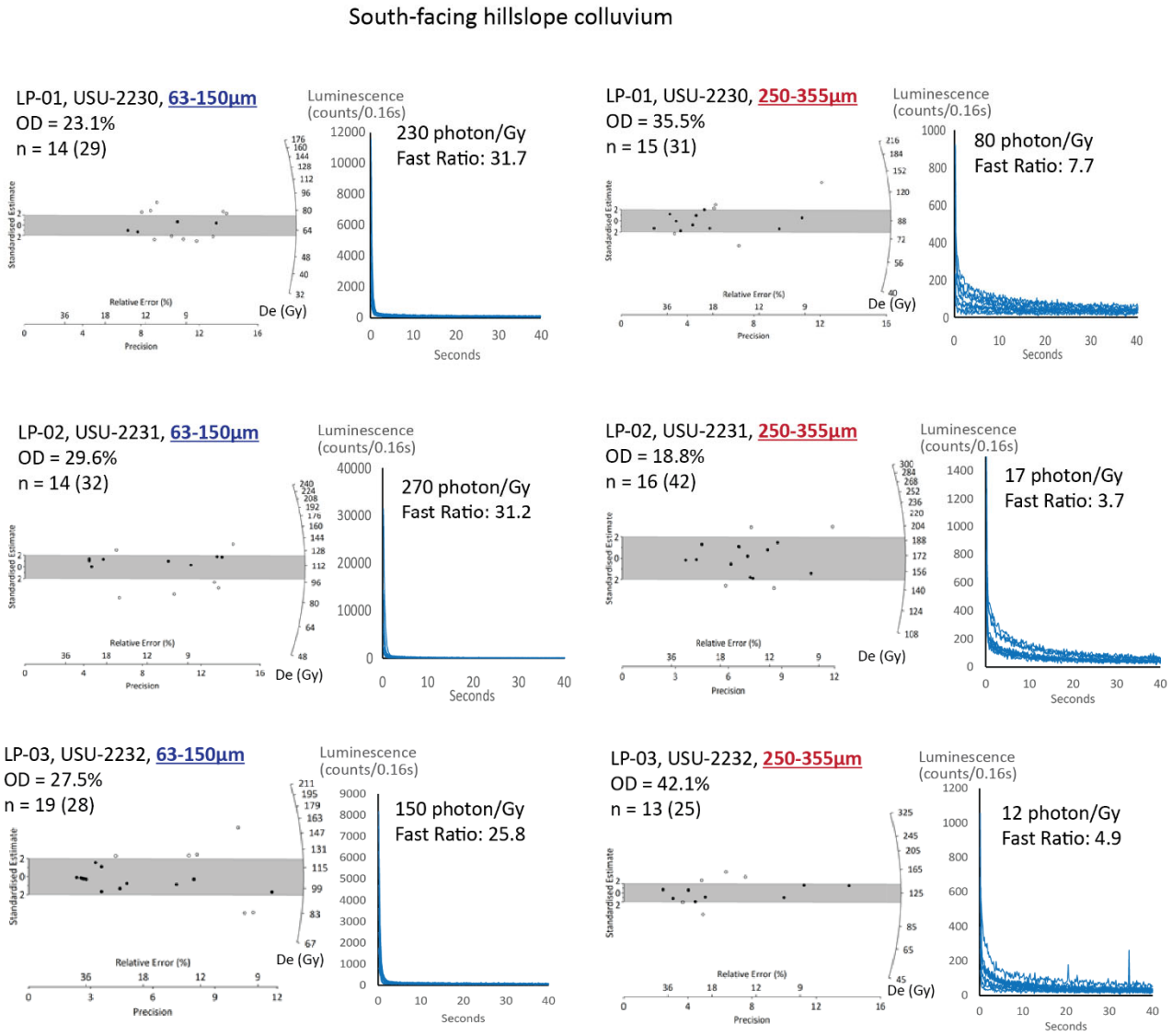

Figure S1. Equivalent dose distributions and the natural luminescence signal decay curves for sample from south-facing hillslope colluvium, plotted in stratigraphic order. The very fine sand fraction is plotted on the left and the fine to medium sand fraction are plotted on the right. Note that the very fine sand fractions have much brighter luminescence signals with greater luminescence sensitivity (number of photon/Gy dose) and higher Fast ratios (Durcan and Duller, 2011), both indicating the grains were likely more distally sourced.

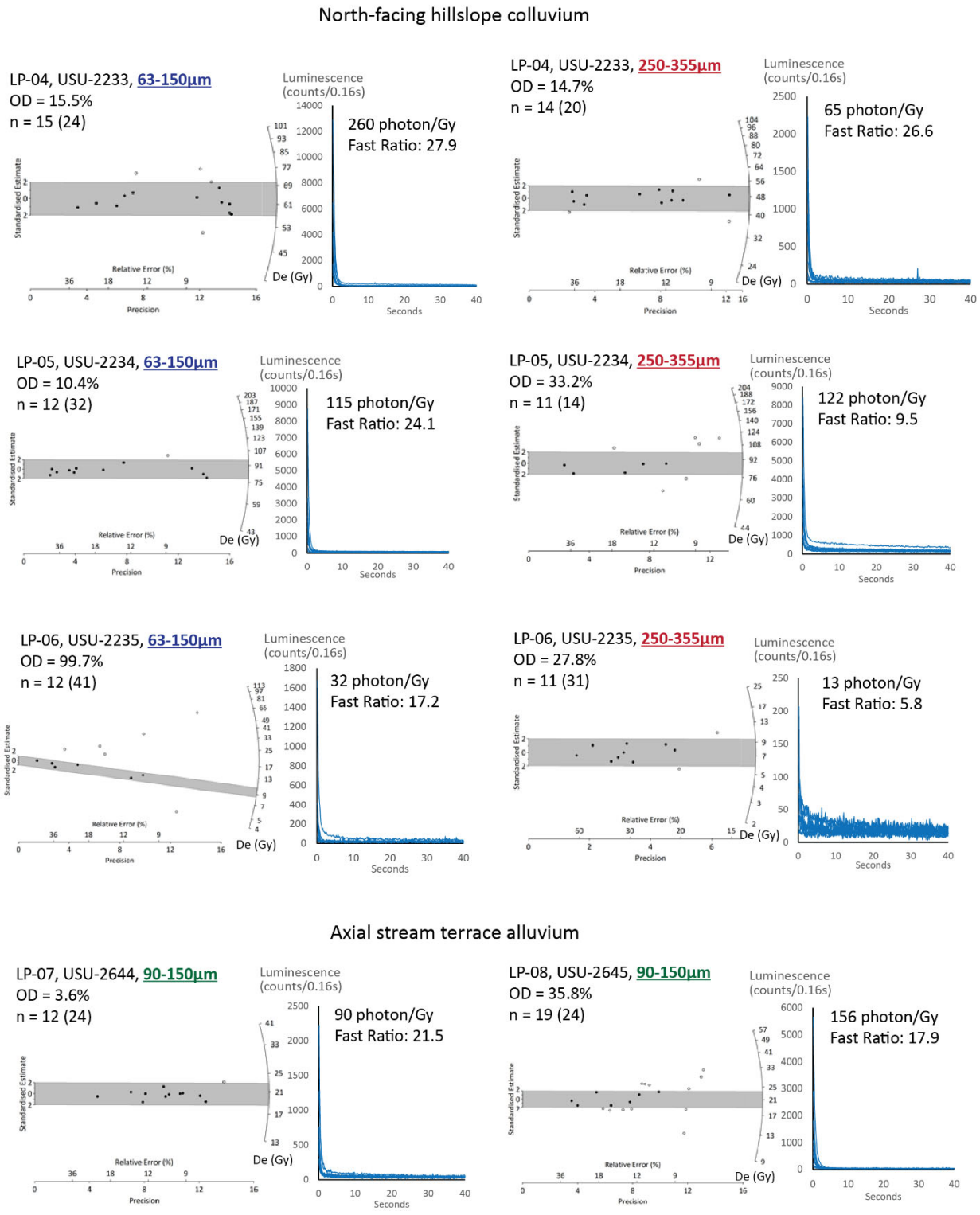

Figure S2. Similar to Figure S1 but with samples from north-facing hillslope colluvium and axial stream terrace alluvium. As with Figure S1, the samples are plotted in stratigraphic order and the coarser sediment are on the right (note that the two stream terrace alluvium samples have the same grain-size).

Laser Diffraction Sample Preparation and Analysis

Particle size of the fine fraction of the soil horizons was determined using laser diffraction (Al-Hashemi et al., 2021; Faé et al., 2019). Roots were removed from samples and then the samples were dried at 105° in an oven. Samples were homogenized and sieved to collect the < 2mm size fraction. Samples were treated with H_2O_2 at 70° C for several hours to remove organic material. Grain size distributions were determined using a Malvern Mastersizer 3000 with a Hydro LV wet dispersion unit. Before and during measurements, samples were ultrasonicated to keep particles disaggregated. To increase accuracy, two different subsamples were analyzed for each soil horizon and the results were averaged.

XRF Sample Preparation and Analysis

XRF samples were analyzed from B-horizons of the hillslope soils. On the north-aspect hillslope, two Btk horizons and one Bk were selected and on the south hillslope the Bk and Btk horizons were sampled (Table S5). Samples were separated into four grain size fractions: 25-125 μm, 125-355 μm, 355-850 μm, and 850-2000 μm by wet sieving the bulk sample. Grains smaller than 25 μm were lost during the wet sieving process. Each grain size fraction was dried in an oven at 105° for one hour. Samples were powdered via a rod and ball mill pulverizer to minimize x-ray fluorescence analysis error. Between 15-25 grams of each sample was pulverized for 5 minutes. Differences in the amount of sample pulverized for analysis resulted from limited quantities of certain grain size fractions. The 25-125 μm and 355-850 μm size size fractions were selected for analysis. For soil horizon Bw at O-S and horizons Bw and Btk2 O-N, the 355-850 μm and 850-2000 μm size fractions were combined due to lack of material to provide accurate results. Samples were analyzed on a Rigaku ZSX Primus II wavelength dispersive XRF spectrometer at the Analytical Geochemistry Laboratory at the University of New Mexico.

Table S5. XRF-Chemistry Information

No.	Component	Result	Unit	Det. Limit	El. Line	Intensity	w/o Normal
Sample: O-S Btk 25-125 µm							
1	Na2O	1.18	mass %	0.01309	Na-KA	4.3257	0.8819
2	MgO	2.35	mass %	0.01077	Mg-KA	21.1996	1.7569
3	Al2O3	18.8	mass %	0.01403	Al-KA	409.7206	14.0187
4	SiO2	57.6	mass %	0.02122	Si-KA	964.2552	43.0149
5	P2O5	0.447	mass %	0.00318	P-KA	12.4370	0.3337
6	SO3	0.0425	mass %	0.00294	S-KA	0.9959	0.0317
7	Cl	0.0131	mass %	0.00382	Cl-KA	0.1955	0.0098
8	K2O	4.06	mass %	0.00447	K-KA	235.5496	3.0293
9	CaO	5.39	mass %	0.00451	Ca-KA	212.3651	4.0252
10	TiO2	1.22	mass %	0.00875	Ti-KA	10.9796	0.9081
11	MnO	0.176	mass %	0.0052	Mn-KB1	7.1322	0.1316
12	Fe2O3	8.39	mass %	0.00627	Fe-KA	470.9443	6.2619
13	NiO	0.0070	mass %	0.00297	Ni-KA	0.6553	0.0053
14	CuO	0.0118	mass %	0.0026	Cu-KA	1.4503	0.0088
15	ZnO	0.0259	mass %	0.00228	Zn-KA	4.3312	0.0194
16	Rb2O	0.0224	mass %	0.00132	Rb-KA	13.2018	0.0167
17	SrO	0.0619	mass %	0.00134	Sr-KA	38.6713	0.0462
18	ZrO2	0.0874	mass %	0.00898	Zr-KB1	12.7516	0.0653
19	Nb2O5	0.0053	mass %	0.00166	Nb-KA	3.4366	0.0039
20	BaO	0.126	mass %	0.02887	Ba-LA	0.5020	0.0940
21	PbO	0.0153	mass %	0.00400	Pb-LA	2.0877	0.0114
Sample: O-S Btk 355-850 µm							
1	Na2O	1.35	mass %	0.01204	Na-KA	5.1990	1.0592
2	MgO	1.34	mass %	0.00942	Mg-KA	12.7462	1.0521
3	Al2O3	17	mass %	0.01283	Al-KA	397.9782	13.3633
4	SiO2	58.8	mass %	0.02045	Si-KA	1070.452	46.3018
5	P2O5	0.609	mass %	0.00327	P-KA	18.0907	0.4796
6	SO3	0.0137	mass %	0.00283	S-KA	0.3435	0.0108
7	Cl	0.0120	mass %	0.00362	Cl-KA	0.1900	0.0094
8	K2O	5.50	mass %	0.00496	K-KA	336.6078	4.3297
9	CaO	6.57	mass %	0.00471	Ca-KA	263.3994	5.1779
10	TiO2	1.10	mass %	0.01373	Ti-KA	9.9725	0.8698
11	MnO	0.206	mass %	0.00513	Mn-KB1	8.4262	0.1623
12	Fe2O3	7.26	mass %	0.00588	Fe-KA	413.3753	5.7157
13	NiO	0.0071	mass %	0.00280	Ni-KA	0.06598	0.0056
14	ZnO	0.0182	mass %	0.00207	Zn-KA	3.2018	0.0144

15	Rb2O	0.0292	mass %	0.00126	Rb-KA	18.1204	0.0230
16	SrO	0.0532	mass %	0.00128	Sr-KA	35.0739	0.0419
17	Y2O3	0.0195	mass %	0.00705	Y-KB1	3.0062	0.0154
18	ZrO2	0.0459	mass %	0.00821	Zr-KB1	7.0648	0.0361
19	BaO	0.0901	mass %	0.03207	Ba-LA	0.3595	0.0710
20	PbO	0.0152	mass %	0.00376	Pb-LA	2.1855	0.0119
Sample: O-S Bk 25-125 µm							
1	Na2O	1.44	mass %	5.4117	Na-KA	5.4117	1.1005
2	MgO	2.36	mass %	21.7179	Mg-KA	21.7179	1.7993
3	Al2O3	18.6	mass %	413.4449	Al-KA	413.4449	14.1436
4	SiO2	58.2	mass %	995.6221	Si-KA	995.6221	44.3446
5	P2O5	0.537	mass %	15.2254	P-KA	15.2254	0.4096
6	SO3	0.0459	mass %	1.0918	S-KA	1.0918	0.0349
7	Cl	0.0155	mass %	0.2343	Cl-KA	0.2343	0.0118
8	K2O	4.18	mass %	247.1712	K-KA	247.1712	3.1877
9	CaO	4.59	mass %	184.2085	Ca-KA	184.2085	3.4983
10	TiO2	1.27	mass %	11.8427	Ti-KA	11.8427	0.9663
11	Cr2O3	0.0147	mass %	0.3695	Cr-KA	0.3695	0.0112
12	MnO	0.137	mass %	6.1670	Mn-KB1	6.167	0.1043
13	Fe2O3	8.35	mass %	94.2582	Fe-KB1	94.2582	6.3656
14	NiO	0.0077	mass %	0.7433	Ni-KA	0.7433	0.0059
15	CuO	0.0056	mass %	0.8175	Cu-KA	0.8175	0.0043
16	ZnO	0.0266	mass %	4.6004	Zn-KA	4.6004	0.0203
17	Rb2O	0.0221	mass %	13.4871	Rb-KA	13.4871	0.0168
18	SrO	0.0648	mass %	41.9411	Sr-KA	41.9411	0.0494
19	ZrO2	0.0848	mass %	12.8064	Zr-KB1	12.8064	0.0646
20	Nb2O5	0.0045	mass %	3.0744	Nb-KA	3.0744	0.0035
21	BaO	0.0852	mass %	0.3518	Ba-LA	0.3518	0.0650
22	PbO	0.0101	mass %	1.4266	Pb-LA	1.4266	0.0077
Sample: O-S Bk 355-2000 µm							
1	Na2O	1.7	mass %	0.0114	Na-KA	6.6952	1.3544
2	MgO	1.41	mass %	0.00953	Mg-KA	13.6736	1.1254
3	Al2O3	17.2	mass %	0.01281	Al-KA	408.5441	13.7082
4	SiO2	59.8	mass %	0.02047	Si-KA	1100.53	47.7082
5	P2O5	0.645	mass %	0.00318	P-KA	19.2432	0.5145
6	SO3	0.0223	mass %	0.00278	S-KA	0.5596	0.0178
7	Cl	0.0120	mass %	0.00349	Cl-KA	0.1909	0.0095
8	K2O	5.66	mass %	0.00369	K-KA	348.7727	4.5203
9	CaO	4.90	mass %	0.00447	Ca-KA	198.1625	3.9099
10	TiO2	1.16	mass %	0.00903	Ti-KA	10.8631	0.9224

11	MnO	0.129	mass %	0.00492	Mn-KA	5.4869	0.103
12	Fe2O3	7.05	mass %	0.00562	Fe-KA	417.6449	5.6278
13	ZnO	0.0151	mass %	0.00199	Zn-KA	2.7637	0.012
14	Rb2O	0.0266	mass %	0.00122	Rb-KA	17.2887	0.0213
15	SrO	0.0447	mass %	0.00125	Sr-KA	30.7922	0.0357
16	ZrO2	0.0497	mass %	0.00799	Zr-KB1	8.0199	0.0397
17	Nb2O5	0.0040	mass %	0.00149	Nb-KA	2.8792	0.0032
18	BaO	0.140	mass %	0.02679	Ba-LA	0.5820	0.1119
19	WO3	0.0209	mass %	0.00622	W-LA	1.1556	0.0167
20	PbO	0.0077	mass %	0.00363	Pb-LA	1.1617	0.0062
Sample: O-N Btk 1 25-125 µm							
2	MgO	2.02	mass %	0.01055	Mg-KA	19.0697	1.5474
3	Al2O3	18.8	mass %	0.01371	Al-KA	430.2213	14.3884
4	SiO2	60.3	mass %	0.02116	Si-KA	1049.837	46.1596
5	P2O5	0.225	mass %	0.00289	P-KA	6.3538	0.1719
6	SO3	0.0393	mass %	0.00281	S-KA	0.9381	0.0301
7	K2O	4.44	mass %	0.00453	K-KA	261.5428	3.3949
8	CaO	4.72	mass %	0.00453	Ca-KA	187.7297	3.6095
9	TiO2	1.05	mass %	0.01041	Ti-KA	9.7248	0.8047
10	Cr2O3	0.0189	mass %	0.00629	Cr-KA	0.4705	0.0145
11	MnO	0.116	mass %	0.03705	Mn-KB1	0.9553	0.0885
12	Fe2O3	6.55	mass %	0.00568	Fe-KA	384.1946	5.0080
13	NiO	0.0087	mass %	0.00271	Ni-KA	0.8891	0.0067
14	CuO	0.0058	mass %	0.00235	Cu-KA	0.8144	0.0044
15	ZnO	0.0190	mass %	0.00205	Zn-KA	3.4833	0.0145
16	Ga2O3	0.0059	mass %	0.00224	Ga-KA	1.1414	0.0045
17	Rb2O	0.0240	mass %	0.00123	Rb-KA	15.6865	0.0184
18	SrO	0.0586	mass %	0.00126	Sr-KA	40.4863	0.0449
19	ZrO2	0.0815	mass %	0.00816	Zr-KB1	13.1684	0.0623
20	Nb2O5	0.0044	mass %	0.00154	Nb-KA	3.1847	0.0034
21	BaO	0.1200	mass %	0.02765	Ba-LA	0.4917	0.0921
Sample: O-N Btk 1 355-850 µm							
1	Na2O	1.45	mass %	0.01105	Na-KA	5.8756	1.1358
2	MgO	0.768	mass %	0.00948	Mg-KA	7.6427	0.5998
3	Al2O3	18.1	mass %	0.01291	Al-KA	443.6889	14.1657
4	SiO2	65.4	mass %	0.02148	Si-KA	########	51.1293
5	P2O5	0.107	mass %	0.00265	P-KA	3.0504	0.0833
6	SO3	0.0197	mass %	0.00272	S-KA	0.4745	0.0154
7	K2O	6.95	mass %	0.00559	K-KA	409.3061	5.4312
8	CaO	2.34	mass %	0.00408	Ca-KA	89.2000	1.8292

9	TiO2	0.464	mass %	0.01012	Ti-KA	4.3318	0.3627
10	MnO	0.166	mass %	0.00461	Mn-KA	7.2486	0.1298
11	Fe2O3	3.96	mass %	0.00500	Fe-KA	242.7436	3.0916
12	NiO	0.0054	mass %	0.00217	Ni-KA	0.7236	0.0042
13	ZnO	0.0083	mass %	0.00191	Zn-KA	1.7119	0.0065
14	As2O3	0.0035	mass %	0.00173	As-KA	1.1157	0.0027
15	Rb2O	0.0381	mass %	0.0011	Rb-KA	28.1955	0.0298
16	SrO	0.0186	mass %	0.00112	Sr-KA	14.6297	0.0145
17	ZrO2	0.0244	mass %	0.00729	Zr-KB1	4.5209	0.0191
18	BaO	0.113	mass %	0.02338	Ba-LA	0.466	0.0884
19	ThO2	0.0041	mass %	0.00201	Th-LA	1.6671	0.0032
Sample: O-N Btk 2 25-125 µm							
1	Na2O	1.44	mass %	0.01261	Na-KA	5.4666	1.0909
2	MgO	2.23	mass %	0.01051	Mg-KA	20.9283	1.6973
3	Al2O3	18.5	mass %	0.0136	Al-KA	419.5797	14.0614
4	SiO2	60.4	mass %	0.02133	Si-KA	########	45.8627
5	P2O5	0.216	mass %	0.00282	P-KA	6.0650	0.1639
6	SO3	0.0359	mass %	0.00289	S-KA	0.8501	0.0273
7	Cl	0.0101	mass %	0.00366	Cl-KA	0.1527	0.0077
8	K2O	4.43	mass %	0.00341	K-KA	259.2984	3.3641
9	CaO	4.88	mass %	0.00435	Ca-KA	192.7650	3.7063
10	TiO2	0.973	mass %	0.01004	Ti-KA	8.9076	0.7391
11	V2O5	0.0292	mass %	0.01009	V-KA	0.5143	0.0222
12	MnO	0.115	mass %	0.00504	Mn-KA	4.7905	0.0871
13	Fe2O3	6.50	mass %	0.00571	Fe-KA	378.7574	4.9363
14	ZnO	0.0162	mass %	0.00213	Zn-KA	2.9470	0.0123
15	As2O3	0.0037	mass %	0.00193	As-KA	1.0567	0.0028
16	Rb2O	0.0231	mass %	0.00122	Rb-KA	14.9898	0.0176
17	SrO	0.0647	mass %	0.00125	Sr-KA	44.5016	0.0492
18	Y2O3	0.0135	mass %	0.00700	Y-KB1	2.1631	0.0102
19	ZrO2	0.0661	mass %	0.00819	Zr-KB1	10.6269	0.0502
20	Bao	0.0983	mass %	0.02912	Ba-LA	0.3978	0.0747
Sample: O-N Btk 2 355-2000 µm							
1	Na2O	1.57	mass %	0.01105	Na-KA	6.1612	1.1823
2	MgO	0.611	mass %	0.00919	Mg-KA	5.8887	0.4591
3	Al2O3	17.1	mass %	0.01285	Al-KA	405.4761	12.8318
4	SiO2	66.7	mass %	0.02179	Si-KA	1202.001	50.1493
5	P2O5	0.0876	mass %	0.00304	P-KA	2.4224	0.0661
6	SO3	0.0277	mass %	0.00291	S-KA	0.6419	0.0208
7	K2O	7.34	mass %	0.00579	K-KA	414.6605	5.5154

8	CaO	2.76	mass %	0.00459	Ca-KA	99.9385	2.0737
9	TiO2	0.317	mass %	0.01105	Ti-KA	2.7904	0.2380
10	MnO	0.133	mass %	0.00474	Mn-KA	5.5227	0.0999
11	Fe2O3	3.15	mass %	0.00501	Fe-KA	184.2615	2.3654
12	NiO	0.0047	mass %	0.00194	Ni-KA	0.7068	0.0035
13	ZnO	0.0058	mass %	0.00192	Zn-KA	1.1735	0.0044
14	Ga2O3	0.0046	mass %	0.00209	Ga-KA	0.9851	0.0035
15	As2O3	0.0039	mass %	0.00179	As-KA	1.2227	0.0029
16	Rb2O	0.0385	mass %	0.00116	Rb-KA	27.9784	0.0289
17	SrO	0.0206	mass %	0.00117	Sr-KA	15.9156	0.0155
18	ZrO2	0.0213	mass %	0.00756	Zr-KB1	3.8912	0.0160
19	BaO	0.108	mass %	0.02862	Ba-LA	0.4217	0.0815

References cited:

Aitken, M.J., 1985. Thermoluminescence Dating. Academic Press, Florida.

Aitken, M. J., 1976, Thermoluminescent age evaluation and assessment of error limits: revised system: Archaeometry, v. 18, p. 233-238.

-, 1985, Thermoluminescence Dating, Florida, Academic Press.

-, 1998, An Introduction to Optical Dating: The dating of Quaternary sediments by the use of photon-stimulated luminescence, New York, Oxford University Press, 267 p.:

Aitken, M. J., and Alldred, J. C., 1972, The assessment of error limits in thermoluminescence dating: Archaeometry, v. 14, p. 257-267.

Al-Hashemi, H. M. B., Al-Amoudi, O. S. B., Yamani, Z. H., Mustafa, Y. M., and Ahmed, H.-U.-R., 2021, The validity of laser diffraction system to reproduce hydrometer results for grain size analysis in geotechnical applications: PloS one, v. 16, no. 1, p. e0245452-e0245452.

Birkeland, P. W., 1999, Soils and Geomorphology, New York, Oxford University Press, 430 p.:

Brennan, B. J., 2003, Beta doses to spherical grains.: Radiation Measurements, v. 37, no. 4-5, p. 299-303.

Colomina, I., and Molina, P., 2014, Unmanned aerial systems for photogrammetry and remote sensing: A review: Isprs Journal of Photogrammetry and Remote Sensing, v. 92, p. 79-97.

Durcan, J. A., and Dulller, G. A., 2011, The fast ratio: a rapid measure for testing the dominance of the fast component in the initial OSL signal from quartz.: Radiation Measurements, v. 46, no. 10, p. 1065-1072.

Faé, G. S., Montes, F., Bazilevskaya, E., Añó, R. M., and Kemanian, A. R., 2019, Making Soil Particle Size Analysis by Laser Diffraction Compatible with Standard Soil Texture Determination Methods: Soil Science Society of America Journal, v. 83, no. 4, p. 1244-1252.

Galbraith, R. F., and Roberts, R. G., 2012, Statistical aspects of equivalent dose and error calculation and display in OSL dating: An overview and some recommendations: Quaternary Geochronology, v. 11, p. 1-27.

Guérin, G., Mercier, N., and Adamiec, G., 2011, Dose-rate conversion factors:update: Ancient TL, v. 29, p. 5-8.

Huntley, D. J., Godfrey-Smith, D. I., and Thewalt, M. L., 1985, Optical dating of sediments: Nature, v. 313, no. 5998, p. 105-107.

Kenworthy, M. K., Rittenour, T. M., Pierce, J. L., Sutfin, N. A., and Sharp, W. D., 2014, Luminescence dating without sand lenses: An application of OSL to coarse-grained alluvial fan deposits of the Lost River Range, Idaho, USA: Quaternary Geochronology, v. 23, p. 9-25.

McAuliffe, J. R., 2016, Perennial Grass-dominated Plant Communities of the Eastern Mojave Desert Region: Desert Plants, v. 32, no. 1, p. 89.

Miller, D. M., and Wooden, J. L., 1993, Geologic map of the New York Mountains area, California and Nevada.

Murray, A. S., and Olley, J. M., 2002, Precision and accuracy in the optically stimulated luminescence dating of sedimentary quartz: a status review: Geochronometria, v. 21, p. 1-16.

Murray, A. S., and Wintle, A. G., 2000, Luminescence dating of quartz using an improved single-aliquot regenerative-dose protocol: Radiation Measurements, v. 32, no. 1, p. 57-73.

Nelson, M. S., Gray, H. J., Johnsone, J. A., Rittenour, T. M., Feathers, J. K., and Mahan, S., 2015, User guide for luminescence sampling in archaeological and geological context: Advances in Archaeological Practice, v. 3, p. 166-177.

Prescott, J. R., and Hutton, J. T., 1994, Cosmic-Ray Contributions to Dose-Rates for Luminescence and Esr Dating - Large Depths and Long-Term Time Variations: Radiation Measurements, v. 23, no. 2-3, p. 497-500.

Rittenour, T. M., Goble, R. J., and Blum, M. D., 2005, Development of an OSL chronology for late Pleistocene channel belts in the lower Mississippi valley: Quaternary Science Reviews, v. 24, p. 2539-2554.

Wintle, A. G., and Murray, A. S., 2006, A review of quartz optically stimulated luminescence characteristics and their relevance in single-aliquot regeneration dating protocols: Radiation Measurements, v. 41, no. 4, p. 369-391.